TECHNICAL NOTE

Comparison between rebinning methods and geometric re-projection for the estimation of missing oblique data in 3D-PET

Fayçal Ben Bouallègue · Jean-François Crouzet · Denis Mariano-Goulart

Abstract

Objective   Classically, the missing portions in the oblique projection data acquired from cylindrical scanners are synthesized by forward projecting an estimation of the activity computed from non-oblique data. Another quick and powerful way to perform the estimation of the truncated portions consists in applying Fourier rebinning methods. This paper intends to compare the performances of 3D geometric re-projection versus two Fourier rebinning techniques (iterative FOREPROJ and extended FORE) designed for re-projection.

Methods   Both analytical and noisy 3D projection data corresponding to a phantom constituted of warm and cold ellipsoids over a uniform background are simulated numerically for the SIEMENS Hi-Rez scanner. The object is reconstructed using 3D filtered back-projection. A prior estimation of the missing oblique data is performed using the three algorithms.

Results   The resolution properties and noise behavior of the three methods are compared and demonstrate a significant signal to noise ratio improvement using rebinning-based algorithms.

F. Ben Bouallègue (✉) · J.-F. Crouzet
Department of Mathematics, Montpellier Science University,
34095 Montpellier, France
e-mail: faybenb@hotmail.com

J.-F. Crouzet
e-mail: crouzet@math.univ-montp2.fr

D. Mariano-Goulart
Biophysics and Nuclear Medicine Department,
Montpellier Medical University, 34295 Montpellier, France
e-mail: d_mariano-goulart@chu-montpellier.fr

Conclusions   We show that iterative FOREPROJ provides projection data with high accuracy 60% less time than geometric re-projection.

Keywords   Image reconstruction ·
Positron emission tomography · Fourier rebinning ·
Re-projection

Introduction

Most of the three-dimensional positron emission tomography (3D-PET) scanners actually used in routine clinical practice are characterized by a large axial field of view (FOV) and hence by a wide range of oblique angles for the detected photon pairs. However, the cylindrical geometry of the PET scanners leads to the truncation of the recorded oblique projections. 3D analytic reconstruction methods such as 3D filtered back-projection (3D-FBP) require axial shift-invariance of the processed data to perform the Fourier transforms involved. Therefore, the missing oblique data have to be estimated prior to the 3D reconstruction. The classical method for the computation of the missing data consists of a two-dimensional reconstruction (2D-FBP) using the axially shift-invariant non-oblique projections followed by a 3D geometric re-projection (3D-GP) of the reconstructed object [1].

In a previous paper [2], we described two new re-projection algorithms based on iterative or extended rebinning methods (iterative FOREPROJ[1]: IT-FP; extended FORE (see footnote 1): EX-FP). We showed that these algorithms

---

[1] FOREPROJ is an abbreviation for "projection by means of Fourier rebinning". FORE is an abbreviation for "Fourier rebinning". See [3, 4] for a complete description of these algorithms.

provide better sinogram estimations and image recon-structions than the classical FOREPROJ and reverse FORE proposed by Defrise et al. [3, 4], although the FORE approximation shows evident limitations at high tilt angles. However, these two new algorithms have not yet been directly compared to the classical 3D-GP method within the frame of 3D direct PET reconstruction. Thereby, the present paper addresses the comparison between the re-binning-based projectors IT-FP and EX-FP, and the classical 3D-GP with a volume model. The three methods are compared on numerically simulated data before image reconstruction using 3D-FBP.

Materials and methods

Theoretical background

The integral of a radioactive distribution $f(x, y, z)$ along the line of response (LOR) parametrized by a radial (s), an angular (ϕ), an axial (z) and a co-polar (θ) variables is (Fig. 1):

$$p(s, \phi, z, \delta)$$
$$= \int_{-\infty}^{+\infty} \mathrm{d}t \, f(s \cos \phi - t \sin \phi, s \sin \phi + t \cos \phi, z + t\delta) \tag{1}$$

where $\delta = \tan \theta$. A set of projections with constant co-polar angle θ is called a segment and is indexed from 0 ($\theta = 0$) to N ($\theta = \theta_{\max}$).

Due to the cylindrical geometry of the scanner, the coincidences are recorded for a given co-polar angle in the following range (Fig. 2):

$$|z| \leq \frac{L}{2} - \delta R \tag{2}$$
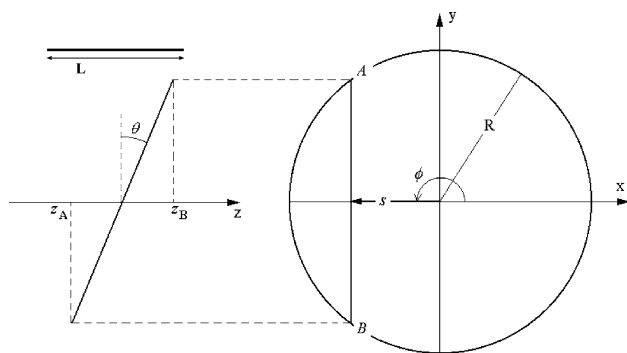
with R the radius of the FOV of the PET scanner.

Fig. 1 Geometry of a PET scanner. *Left* longitudinal section showing the axial variables z and θ. *Right* transaxial view. The standard sinogram variables s and ϕ parameterize the *straight line* AB

However, the projection information lies all over the range:

$$|z| \leq \frac{L}{2} + \delta R \tag{3}$$

Thus, the truncation affects the data in the range:

$$\frac{L}{2} - \delta R < |z| \leq \frac{L}{2} + \delta R \tag{4}$$

Only segment 0 ($\theta = 0$) is axially shift-invariant. Upper segments ($\theta > 0$) must be completed before the application of 3D-FBP. Our goal is to compare the three following methods for the completion of the oblique 3D data (Fig. 3):

Geometric re-projection

The 3D-GP is performed on the basis of a slice-by-slice reconstruction of the object realized with the non-oblique projections by means of a 2D-FBP for each transaxial slice [1]. Denoting f^* the first estimation of the activity f, the
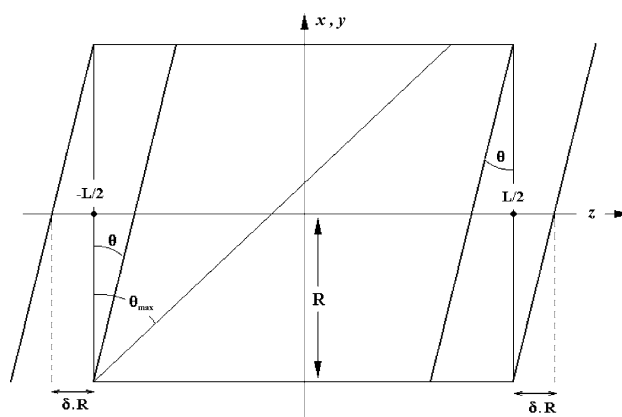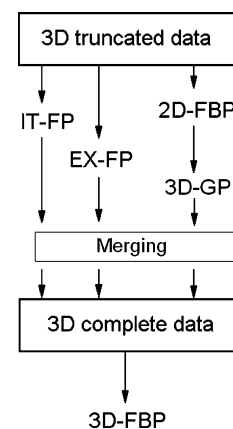

Fig. 2 The problem of the missing projections in the set of measured data: only segment 0 ($\delta = \tan \theta = 0$) is axially shift-invariant. Here, $\theta_{\max} = a \tan(\delta_{\max})$ is the aperture of the scanner, with $\delta_{\max}$ the maximum ring difference

Fig. 3 Diagram for the comparison of the three re-projection methods

missing projections are computed using a geometric projector GP(L, i, j, k):

$$p(s, \phi, z, \delta) = \sum_{i,j,k} \mathrm{GP}(L, i, j, k) f^*(i, j, k) \qquad (5)$$

where the summation runs over the voxel indices (i, j, k) and the index L represents the LOR with parameters (s, ϕ, z, δ). The components of the GP matrix represent the volume of the intersection between the voxel (i, j, k) and the LOR L. It should be noted that the GP matrix is highly sparse, as a given LOR only intersects few of the object voxels. The re-projection algorithm is hence designed to optimize the implementation of Eq. 5 by targeting the non-zero coefficients before the summation.

Iterative FOREPROJ (IT-FP)

The IT-FP method [2] is based on the relation between the 3D Fourier transforms of $p(s, \phi, z, \delta)$ with respect to the first three variables for two different values of δ:

$$\wp(\omega_1, k, \zeta, \delta_1) = \exp(-i\Delta\Phi)\wp(\omega_2, k, \zeta, \delta_2) \qquad (6)$$

$$\omega_1^2 + \zeta^2 \delta_1^2 = \omega_2^2 + \zeta^2 \delta_2^2 \qquad (7)$$

with

$$\begin{aligned}\Delta\Phi &= k\left(a\tan\left(\frac{\zeta\delta_1}{\omega_1}\right) - a\tan\left(\frac{\zeta\delta_2}{\omega_2}\right)\right) \\ &= ka\tan\left(\zeta\frac{\delta_1^2 - \delta_2^2}{\delta_1\omega_1 + \delta_2\omega_2}\right)\end{aligned} \qquad (8)$$

Equation 6 allows the iterative estimation [2] of a missing oblique projection $p(s, \phi, z, \delta)$ given the set $\{p(s, \phi, z, \delta'), \delta' < \delta\}$ (Fig. 4). No radial zero-padding is carried out when applying IT-FP.

Extended FORE (EX-FP)

The EX-FP algorithm [2] links every two segments in the 2D Fourier space:

$$P(\omega, k, z, \delta_1) \approx P\left(\omega, k, z - \frac{k(\delta_1 - \delta_2)}{\omega}, \delta_2\right) \qquad (9)$$

It enables a re-evaluation of any segment on the basis of the entire 3D data set by averaging the right member of Eq. 9 over the whole δ range.

Numerical simulations

For the simulations, we choose a phantom constituted of warm and cold ellipsoids over a uniform background (Fig. 5). The background activity, fixed to 2, is confined into a cylinder of radius 150 mm. A pattern made up of a centered cold ellipsoid of half-axes 60, 60 and 8.3 mm
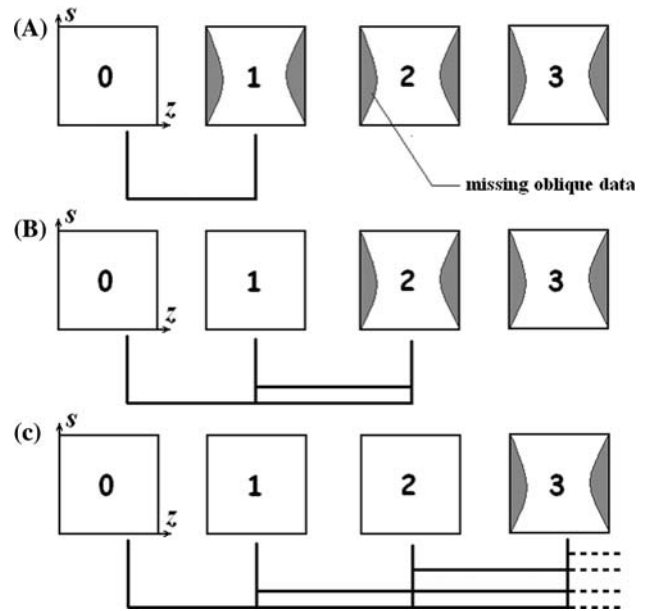

Fig. 4 Flow chart for the computation of IT-FP: *segment 1* is first estimated and completed using *segment 0* (**a**). Then *segment 2* is completed using *segments 0 and 1* (**b**), and the process goes on iteratively until the every segments has been completed (**c**)
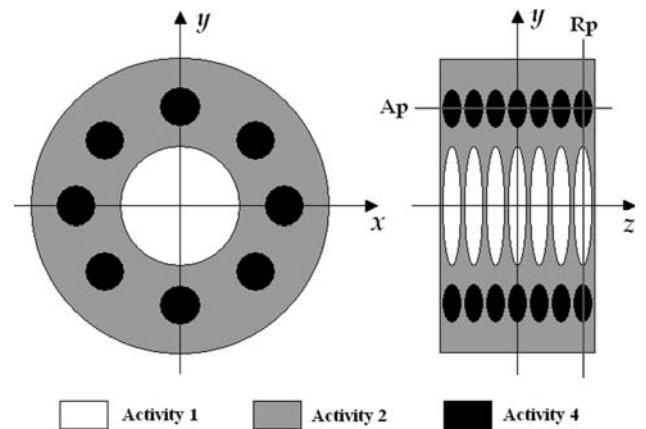

Fig. 5 The studied object is constituted of warm and cold ellipsoids over a uniform background. Here are displayed the (x, y) and the (y, z) views

(activity 1) and eight off-axis warm ellipsoids of half-axes 20, 20 and 8.3 mm (activity 4) is repeated every 22.8 mm along the z axis.

The 3D projection data are simulated analytically [5], assuming no attenuation and equidistant parallel projections, for the SIEMENS Hi-Rez scanner, which is approximated as a 39 ring-scan with a diameter of 823 mm. Each ring is made up of 624 detectors of size 4 mm. The axial FOV is 161.85 mm and the transverse FOV radius is 321.6 mm. The maximum ring difference is fixed to 31 and the axial compression (span) to 3, hence leading to an aperture of 8.6° and 11 values for the azimuthal tilt angle θ

of the recorded coincidences (11 segments, segment 0 corresponding to the transverse projections).

The initial sampling of the 2D sinograms for the SIE-MENS Hi-Rez scan is 312 × 312. These sinograms are re-sampled to 128 × 128 in order to carry out the fast Fourier transforms (FFTs), which lead to a pixel size of 5×5 mm^2. The axial sampling is conserved: the transverse projections are constituted of 77 slices, which correspond to a slice thickness of 2.075 mm. Zero-padding is achieved in the axial direction in order to bring the number of samples to 128.

Besides the noiseless simulation, Poisson noise is introduced into the data [5] in order to study the noise behavior of the algorithms. The total of the simulated net trues ranges 100–400 Mcounts. In these two sets of projections, the noiseless ones and the noisy ones, there are missing oblique data, as the software only simulates the data really acquired by the scanner.

In order to judge the quality of the three methods in estimating these missing oblique data, we analytically compute the whole set of complete 3D projections, called in what follows 'exact data'.

The oblique projections corresponding to segments 1–10 are estimated for both noiseless and noisy data using the three methods. Concerning 3D-GP, the prior 2D-FBP reconstruction is performed using a ramp filter implemented either with a cut-off at 60% of the Nyquist

frequency or without cut-off. These two implementations are, respectively, referred to in what follows as 3D-GP-60% and 3D-GP-100%. The estimated oblique projections are compared with the exact data for segments 2, 6 and 10.

After the estimation stage, the calculated projections are merged with the simulated ones in the range $|z| > (L/2) - \delta R$. The completed data are then used to run 3D-FBP. When processing noisy data, the frequency cut-off of the Colsher filter is fixed to 60% of the Nyquist frequency. When processing noiseless data, no cut-off is applied to the Colsher filter.

When performing 2D- or 3D-FBP, the image matrix has a size of 128 × 128 × 128 corresponding to a voxel size of $5 \times 5 \times 2.075$ mm^3.

Results and discussion

Figures 6 and 7 show the histograms of the pixel difference (in absolute value) between the exact sinograms and the sinograms estimated (computed from the whole sinograms, before merging) from both noiseless (Fig. 6) and noisy (Fig. 7, 200 Mcounts) data. Figure 6 shows that IT-FP provides estimations whose quality in terms of absolute error is comparable to that achieved with 3D-GP, whatever the segment considered. Due to the approximations involved, the results of EX-FP remain acceptable for the
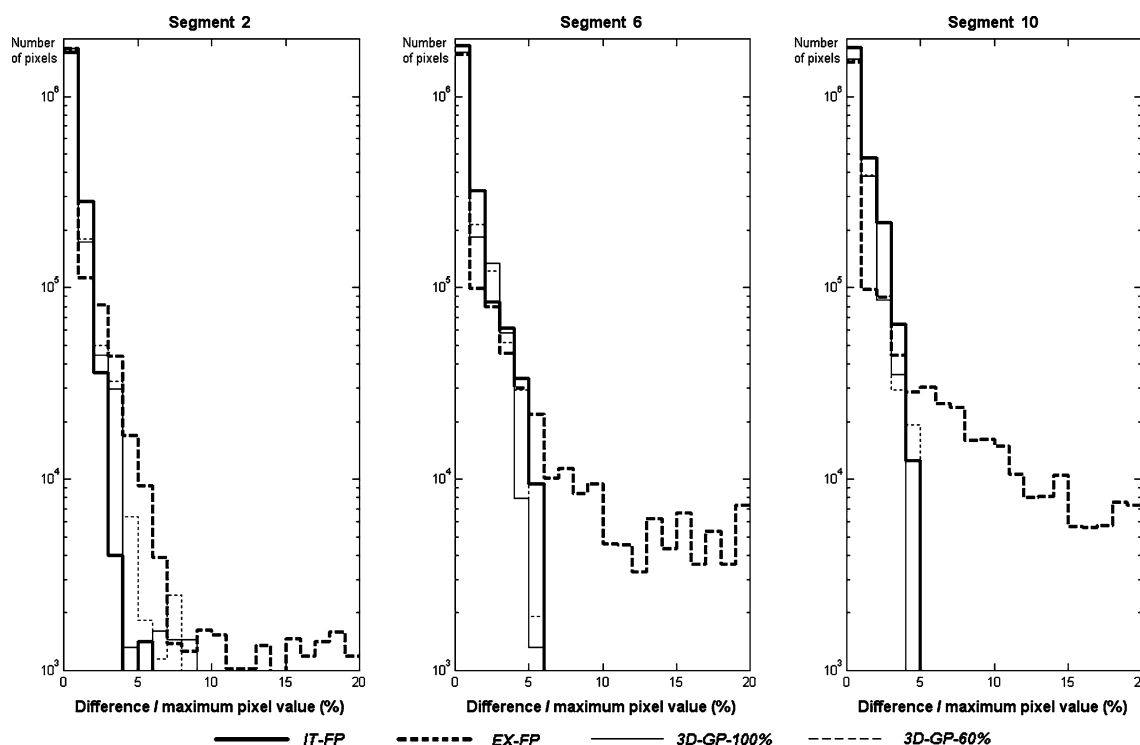

Fig. 6 Histogram of the difference (normalized to the data maximum) between the exact sinograms and the sinograms estimated from noiseless data. Comparison between 3D-GP-60% (dashed), 3D-GP-100% (solid), EX-FP (dashed bold) and IT-FP (solid bold)
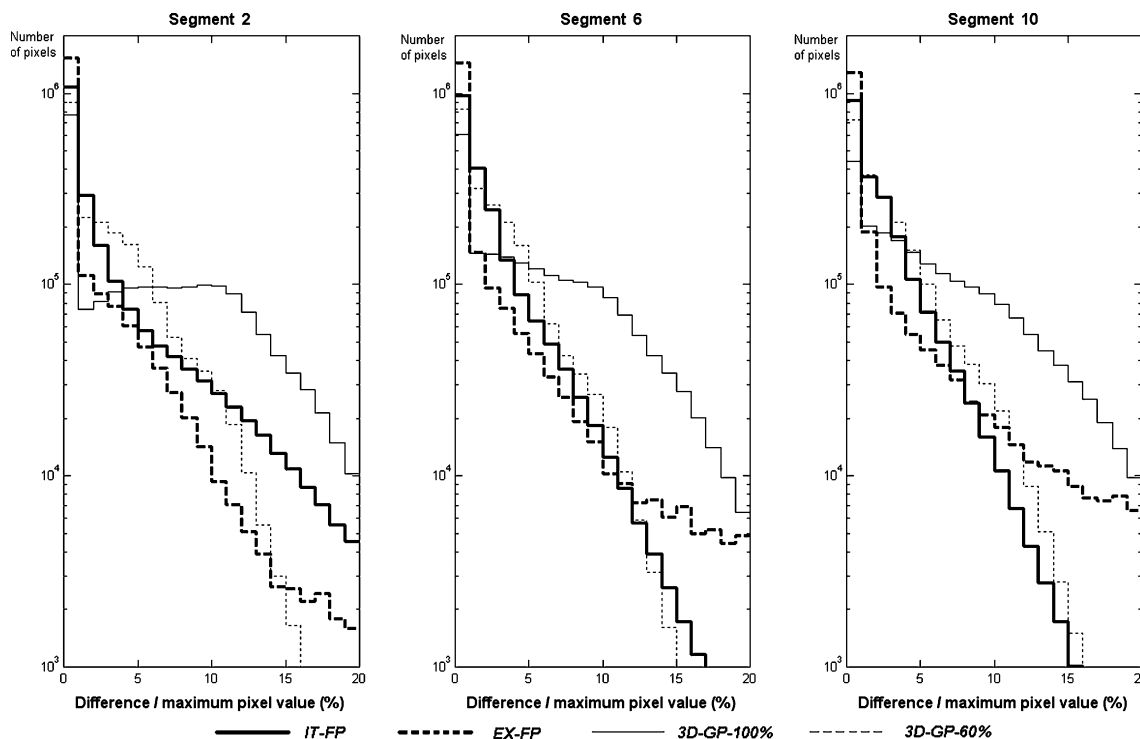
Fig. 7 Histogram of the difference (normalized to the data maximum) between the exact sinograms and the sinograms estimated from noisy data (200 Mcounts). Comparison between 3D-GP-60% (*dashed*), 3D-GP-100% (*solid*), EX-FP (*dashed bold*) and IT-FP (*solid bold*)
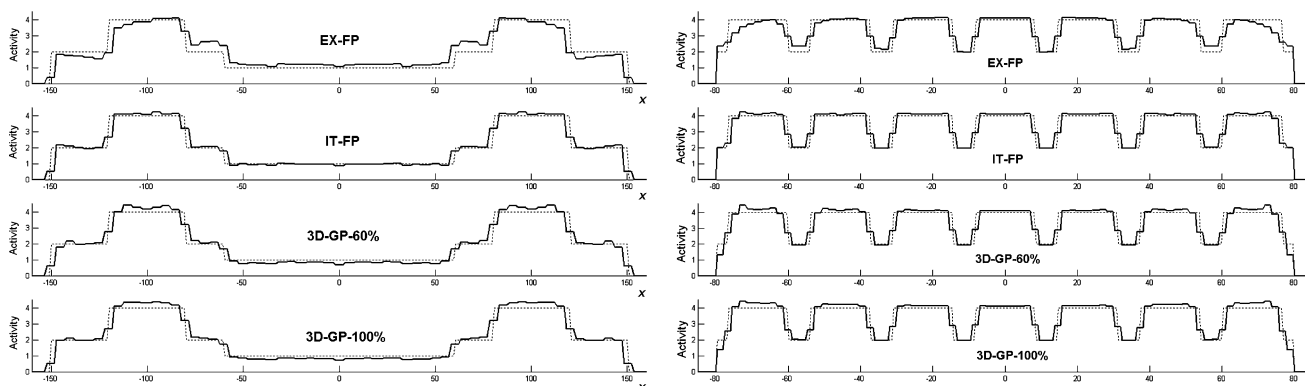

Fig. 8 Radial (*left*) and axial (*right*) line profiles through the object reconstructed from noiseless data. The *dashed curves* correspond to the exact line profile through the object. The completion was achieved using, from *top* to *bottom*: EX-FP, IT-FP, 3D-GP-60% and 3D-GP-100%

first segments but quickly deteriorate with the co-polar angle of the computed projections. Figure 7 shows clearly that the data estimated with EX-FP and IT-FP are more reliable than those estimated with 3D-GP-100% when working with realistic noisy data. The quality of the sinograms computed with the rebinning methods is equivalent to that achieved with 3D-GP-60%. Due to the iterative implementation, the results obtained with IT-FP tend to improve with the segment index. Inversely, because of an increasing systematic error, the quality of the EX-FP estimations decreases with the segment index.

Figure 8 shows radial (left) and axial (right) line profiles through the object reconstructed from noiseless data and exhibits the intrinsic influence of each method on the spatial resolution. The profiles are extracted through line Rp and line Ap shown in Fig. 5. They attest that there is no resolution loss when using IT-FP compared with the resolution recovery achieved with 3D-GP. Moreover, the axial line profiles show that IT-FP leads to fewer partial volume effects in the external slices. As for EX-FP, it exhibits axial smoothing due to axial interpolations following from Eq. 9 as well as radial distortions
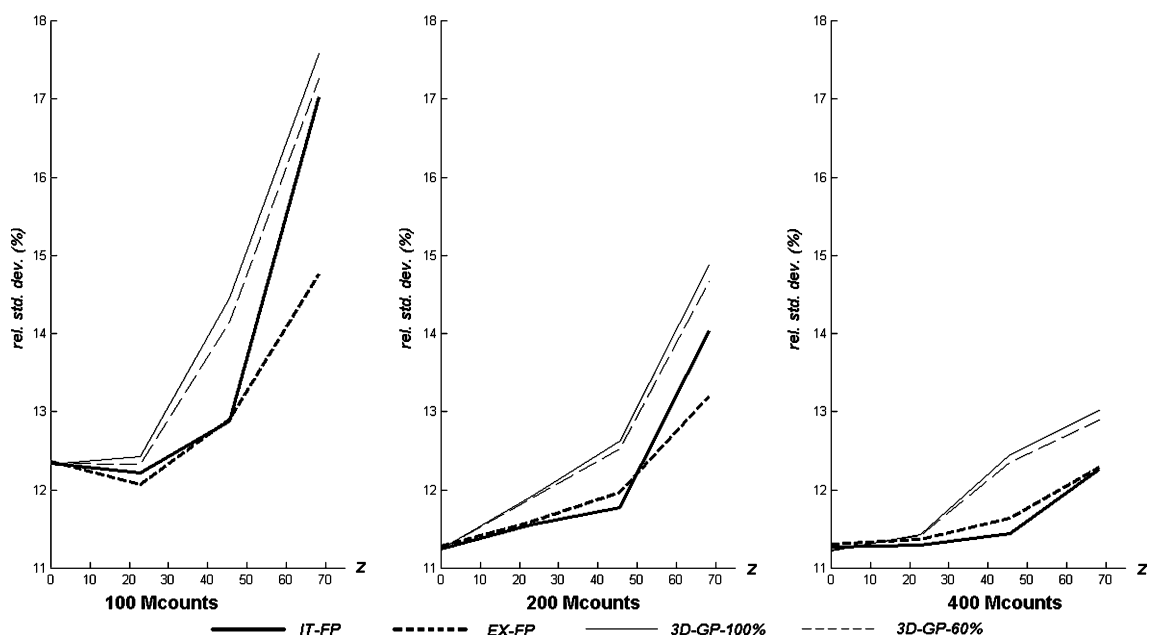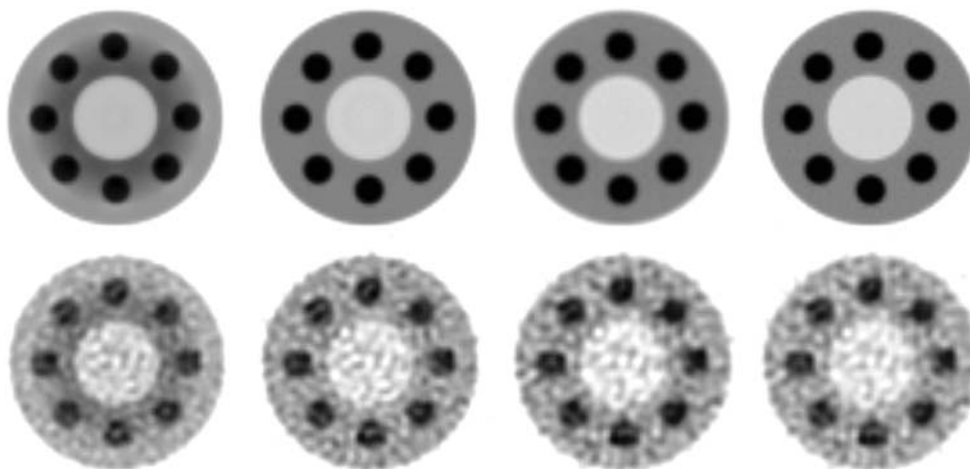
Table 1 Representative computational costs

Method	Computation time (s)
EX-FP	45
IT-FP	120
2D-FBP + 3D-GP	80 + 210 = 290

time for the computation of the GP matrix which is computed once and stored on hard disk for further exploitation. It appears that the processing time is 2.4 times longer with 3D-GP than with IT-FP. As analytical reconstructions are chosen generally because they perform faster than iterative methods, the faster execution time of IT-FP followed by 3D-FBP may be of prime importance when fast 3D reconstructions are required.

Conclusions

We performed a systematic comparison between 3D-GP and two Fourier rebinning algorithms designed for the solution of the data truncation problem (IT-FP and EX-FP), including quality of the estimated segments, resolution properties and noise behavior. EX-FP exhibits significant standard deviation reduction compared with 3D-GP. However, as it implies the same axial approximation as FORE does, it leads to artifacts in the estimated segments resulting in loss of resolution and distortion in the reconstructed volumes. For IT-FP, the quality of the estimated segments is equivalent to that of 3D-GP when working with noiseless data. When working with noisy data, the quality of the estimated sinograms in terms of absolute error is comparable to that achieved with 3D-GP. In addition, IT-FP allows 3D reconstructions with fewer partial volume effects in the external slices and similar axial resolution in 60% less time.

References

1. Kinahan PE, Rogers JG. Analytic three-dimensional image reconstruction using all detected events. IEEE Trans Nucl Sci. 1990;36:964–8.
2. Ben Bouallègue F, Crouzet JF, Comtat C, Fourcade M, Mohammadi B, Mariano-Goulart D. Exact and approximate Fourier rebinning algorithms for the solution of the data truncation problem in 3D PET. IEEE Trans Med Imag. 2007;26–7:1001–9.
3. Defrise M, Kinahan PE, Townsend DW, Michel C, Sibomana M, Newport DF. Exact and approximate rebinning algorithms for 3-D PET data. IEEE Trans Med Imag. 1997;16:145–58.
4. Liu X, Defrise M, Michel C, Sibomana M, Comtat C, Kinahan PE, et al. Exact rebinning methods for three-dimensional positron tomography. IEEE Trans Med Imag. 1999;18:657–64.
5. Comtat C, Kinahan P, Defrise M, Michel C, Lartizien C, Townsend D. Simulating whole-body PET scanning with rapid analytical methods. In: Proceedings of IEEE Nuclear Science Symposium and Medical Imaging Conference, Seattle, WA, 1999. Piscataway, NJ: IEEE; 2000, p. M7-83.